ORIGINAL RESEARCH

Phosphoglycerate Dehydrogenase Overexpression Inhibits Ferroptosis to Repress Calcification of Human Coronary Artery Vascular Smooth Muscle Cells via the P53/SLC7A11 Pathway

Yuhai Zou[1,*], Dongdong Li[1,*], Ge Guan[1], Wenting Liu[2]

[1]Department of Cardiology, General Hospital of Southern Theatre Command of PLA, Guangzhou, 510010, People's Republic of China; [2]Department of Otorhinolaryngology, Guangzhou First People's Hospital, Guangzhou, 510180, People's Republic of China

*These authors contributed equally to this work

Correspondence: Wenting Liu, Department of Otorhinolaryngology, Guangzhou First People's Hospital, Guangzhou, 510180, People's Republic of China, Tel +86-13533976302, Email liuwt2023@126.com

Background: Coronary artery calcification (CAC) is in almost all patients with coronary artery disease and requires more effective therapies. We aim to explore the effects of phosphoglycerate dehydrogenase (PHGDH) on CAC.
Methods: We identified the differentially expressed genes through bioinformatic analysis and selected PHGDH for further verification. Human coronary artery smooth muscle cells (HCASMCs) cultured with calcifying medium were used as models of CAC in vitro. Erastin was administered to induce ferroptosis. We determined the cell viability by the cell count kit-8 assay. The alkaline phosphatase activity, calcium content, and the expression of glutathione were evaluated by the corresponding detection kits. The calcification level was detected by alizarin red staining. Then we performed Western blot to examine the expression of runt-related transcription factor 2, bone morphogenetic protein 2, cyclooxygenase 2, glutathione peroxidase 4, P53, and solute carrier family 7a member 11 (SLC7A11).
Results: We acquired 201 differentially expressed genes and selected PHGDH to verify. In calcifying medium-induced HCASMCs, PHGDH overexpression increased the cell viability and decreased the alkaline phosphatase activity, calcium content, calcification level, and the expression of bone morphogenetic protein 2 and runt-related transcription factor 2. Additionally, we found higher levels of glutathione, glutathione peroxidase 4, and SLC7A11 and lower levels of cyclooxygenase 2 and P53 after up-regulating PHGDH. Erastin reversed the effects of PHGDH on calcification of HCASMCs.
Conclusion: PHGDH overexpression suppresses the calcification level of HCASMCs by inhibiting ferroptosis through the P53/SLC7A11 signaling pathway, suggesting PHGDH as a promising therapeutic target of CAC.
Keywords: coronary artery calcification, PHGDH, the P53/SLC7A11 signaling pathway

Introduction

Coronary artery calcification (CAC) is a process of vascular degeneration in which calcium deposits occur within the coronary artery vessel wall.[1] CAC is common in all patients with coronary artery disease and is affected by multiple factors such as age, gender, and race.[1] CAC begins as microcalcification (0.5 ~ 15 μm), then grows into larger calcium fragments, and finally leads to sheet-like deposits (> 3 mm),[2] which is closely related to the development of atherosclerosis, the extent of coronary heart disease and long-term mortality independent of conventional risk factors.[3–5] Currently, as there are few definitive pharmacological interventions available, CAC is primarily treated through interventional procedures like coronary artery rotational atherectomy,[6,7] with a high rate of postoperative complications. It is urgent to search for biomarkers that can be used for effective diagnosis and treatment of CAC.

3673

Phosphoglycerate dehydrogenase (PHGDH) is a kind of rate-limiting enzyme in the first step of the serine synthesis pathway, involved in multiple types of diseases. Increasing evidence has demonstrated that PHGDH is associated with supporting cancer growth, proliferation, and metastasis[8–10] and also mediates tumor resistance.[11,12] Chen X et al have reported that PHGDH expression is positively correlated with the progression of Alzheimer's disease pathology and symptoms.[13] PHGDH overexpression serves a protective role in osteoarthritis by promoting extracellular matrix synthesis and decreasing the levels of inflammation, apoptosis, and oxidative stress.[14] In cardiovascular diseases, Perea-Gil et al have found that PHGDH plays a role in the rescue of dilated cardiomyopathy phenotypes.[15] Truong V et al have reported that the epigenetic regulation of the PHGDH is associated with blood triglyceride metabolism in venous thromboembolism.[16] In addition, PHGDH inhibits vascular endothelial cell senescence by elevating the stability and activity of pyruvate kinase M2.[17] However, whether PHGDH has an effect on CAC is unknown.

A growing number of studies have found PHGDH can play a role in different diseases by regulating ferroptosis which is a kind of programmed cell death driven by iron-dependent phospholipid peroxidation.[18,19] In bladder cancer, PHGDH is up-regulated and promotes the progression of cancer by suppressing ferroptosis.[20] In prostate cancer, down-regulation of PHGDH induces ferroptosis and reverses enzalutamide resistance.[12] Notably, many subtypes of cardiovascular disease are associated with iron imbalance, suggesting ferroptosis as a promising treatment target for cardiovascular diseases. For instance, the restraint of ferroptosis of vascular smooth muscle cells alleviates atherosclerosis.[21] Inhibition of acyl-coenzyme A thioesters synthetase long-chain family member 4 protects against ischemia/reperfusion injury by suppressing ferroptosis.[22] Mitochondrial outer membrane protein hepatitis C virus core binding protein 6 stimulates ferroptosis, leading to doxorubicin-induced cardiomyopathy.[23] However, whether PHGDH can regulate ferroptosis in CAC needs to be further investigated.

Recently, bioinformatics methods have been often used to identify potential biomarkers and therapeutic targets of cardiovascular diseases.[24–26] Therefore, bioinformatic analysis was conducted in this study to explore the differentially expressed genes (DEGs). We selected PHGDH to verify and found that up-regulation of PHGDH could alleviate the calcification of human coronary artery smooth muscle cells (HCASMCs), in hopes of providing more insights into the diagnosis and treatment of CAC.

Materials and Methods

Identification of DEGs

The Gene Expression Omnibus (GEO) database (https://www.ncbi.nlm.nih.gov/geo/) was used to download the gene expression profiling. Taking "coronary artery calcification" as a keyword to screen, we then selected the GSE211722 dataset. To identify the DEGs between CAC samples and controls, we used GEO2R (www.ncbi.nlm.nih.gov/geo/geo2r) and set | logFC| ≥ 1.7 and adjusted p ≤ 0.05 as the thresholds. Boxplots then were conducted for data correction and standardization and volcano plots were used to visualize the DEGs. The gene set enrichment analysis was performed for pathway enrichment analysis and the top 15 up-regulated genes and the top 15 down-regulated genes were shown in a heatmap.

Functional and Pathway Enrichment Analysis

In order to conduct Gene Ontology (GO) and Kyoto Encyclopedia of Genes and Genomes (KEGG) pathway analysis, we submitted the DEGs to the Database for Annotation, Visualization, and Integrated Discovery (https://david.ncifcrf.gov/summary.jsp), and displayed the top 8 items in the enrichment analysis column diagram and the bubble diagram.

Construction of the Protein-Protein Interaction (PPI) Network and Acquisition of Hub Genes

Using the Search Tool for the Retrieval of Interacting Genes Database (https://www.string-db.org/), we acquired the information on interactions between proteins encoded by DEGs, setting the confidence interaction score at 0.4. Then the Cytoscape software (www.cytoscape.org/) was used to show the PPI network and hub genes were screened out using the plug-ins CytoHubba1 and Molecular Complex Detection.

Hub Gene Analysis

Firstly, we drew the expression ridgeline plot to show the distribution of genes in different sample data. Then we conducted the principal component analysis (PCA) to observe whether the hub genes we selected could distinguish the patients with CAC from healthy patients. A chordal graph was performed to reveal the expression changes of hub genes involved in the GO terms and a matrix analysis diagram was used to show the internal correlation of hub genes in GSE211722. Finally, the diagnostic accuracy of hub genes was evaluated by receiver operating characteristic (ROC) curves, which were drawn by Gene Expression Profile Interactive Analysis (http://gepia.cancer-pku.cn/).

CAC Model in vivo

We purchased 7-8-week-old male DBA-2J mice weighing 18~20 g from SPF (Beijing) Biotechnology Co., Ltd. (Beijing, China). The animals were randomly classified into the Control group and the CAC group, containing 6 mice in each group. The mice in the CAC group were administered a warfarin-containing diet (3 mg warfarin/g diet and 1.5 mg vitamin K1/g diet) to induce vascular calcification while the mice in the control group were fed a normal diet until mice were sacrificed.[27] After 8 weeks, cervical dislocation was conducted to kill mice for collection of blood and myocardial tissues. All animal experimental procedures were performed with the approval of the Animal Care and Use Committee (Approval No.: SYDW2023070).

Hematoxylin and Eosin (H&E) Staining and Von-Kossa Staining

The myocardial tissue samples were embedded in paraffin after being fixed in 4% paraformaldehyde, cut into 5 μm, and then stained with Hematoxylin and Eosin to evaluate the pathologic changes of the coronary artery. Calcium deposition in the coronary artery was identified by Von-Kossa staining. All steps were carried out in strict accordance with the instructions of staining kits. The results were analyzed with a microscope (Eclipse 80i, Tokyo, Japan).

Immunofluorescence Co-Staining Analysis

We detected the co-localization of PHGDH and α-smooth muscle actin (α-SMA), the vascular smooth muscle cell marker protein, by dual-color immunofluorescence staining to analyze the relative expression level of PHGDH in aortic smooth muscle cells of CAC mice heart tissue. The sections which were deparaffinized and dehydrated were incubated with primary antibodies at 4°C overnight which included rabbit-anti-α-SMA (ab5831, 1:100, Abcam, Cambridge, USA) and mouse-anti-PHGDH (ab236763, 1:100, Abcam). It was then exposed to secondary antibodies at room temperature for 1 h which included Alexa Fluor 488 goat anti-rabbit IgG (ab150077, 1:100, Abcam) and Alexa Fluor 647 goat anti-mouse IgG (ab150115, 1:100, Abcam). Finally, the sections were incubated with 4',6-diamidino-2-phenylindole (DAPI; ab104139, 1:1000, Abcam). All images were visualized and photographed using a fluorescent microscope under the same parameters.

Cell Culture and Treatment

Primary HCASMCs were purchased from iCell Bioscience Inc. (Shanghai, China). The growth medium for HCASMCs consisted of Dulbecco's modified eagle medium (Gibco, Grand Island, NY, USA) containing 10% fetal bovine serum (FBS, Gibco) and 1% penicillin/streptomycin (Gibco). To induce cell calcification, HCASMCs were cultured in calcifying medium (CM) for 7 days, which was growth medium supplemented with β-glycerophosphate (10 mM, Sigma-Aldrich, St Louis, MO, USA) and calcium chloride (3 mM, Sigma-Aldrich).

The overexpression plasmids PHGDH (pcDNA3.1-PHGDH) or empty plasmid pcDNA3.1-NC were purchased from Shenggong Bioengineering Company (Shanghai, China). The cells with induction of calcification were transfected with the pcDNA3.1-RAD54L or pcDNA3.1-NC using Lipofectamine 2000 (Life Technologies Corporation, Carlsbad, CA, USA) for 48 h to overexpress PHGDH (oe-PHGDH group) or perform as a control (oe-NC group). To investigate the relationship between ferroptosis and PHGDH, ferrostatin-1 (Fer-1, 5mM, MedChemExpress, NJ, USA) was used to inhibit ferroptosis, and Erastin (5mM, MedChemExpress) was administered to induce ferroptosis. To down-regulate the expression of PHGDH, HCASMCs were transfected with small interfering RNA (siRNA) for PHGDH (si- PHGDH) with

the Lipofectamine 2000 kit (Life Technologies Corporation). The si-NC was transfected into cells in the same way as a negative control. Therefore, the cells were grouped as follows: Normal group (HCASMCs without any treatment), Control group, oe-NC group, oe-PHGDH group, Fer-1 group (oe-NC + Fer-1), Erastin group (oe-NC + Erastin), oe-PHGDH + Erastin group, si-NC group, and si-PHGDH group.

Real-Time Quantitative Polymerase Chain Reaction (RT-qPCR)

The relative mRNA expression levels of PHGDH, solute carrier family 6 member 9 (SLC6A9), asparagine synthetase (ASNS), tribbles homologue 3 (TRIB3), solute carrier family 7 member 5 (SLC7A5), and solute carrier family 7 member 1 (SLC7A1) were determined by RT-qPCR. Total RNAs of myocardial tissues or HCASMCs were reversely transcribed into cDNA by the PrimeScript RT Reagent kit (Vazyme, Nanjing, China). RT-qPCR was performed on ABI7500 FAST Real-Time PCR (Applied Biosystems, Foster City, CA, USA) with the condition of 95°C, 30s initial denaturation, and 40 amplification cycles (95°C, 10s, and 60°C, 30s). The mRNA relative expression levels were calculated by the $2^{-\Delta\Delta Ct}$ method using GAPDH as the housekeeping gene. The sequences of primers were listed in Supplementary Table 1.

Cell Count Kit-8 (CCK-8) Assay

HCASMCs from different groups were seeded in 96-well plates at a density of 1.5×10^4 cells/well. After 24 h of culture, 10 μL CCK-8 reagents (Solarbio, Beijing, China) were added to each well with an additional 2 h incubation in the dark condition. Then a microplate reader was used to record the optical density (OD) of each well at 450 nm.

Enzyme-Linked Immunosorbent Assay (ELISA) and Alkaline Phosphatase (ALP) Assay

We determined the expression levels of ALP and runt-related transcription factor 2 (Runx2) in the serum of mice, and the expression level of glutathione (GSH) in the cell supernatant with corresponding ELISA kits (Esebio, Shanghai, China) following the instructions in the manual. Finally, the OD values were recorded under a microplate reader at 450 nm. The cell lysates were collected for ALP enzyme activity determination using an ALP assay kit (Abcam).

Calcium Content Assay

We examined the calcium content with a calcium assay kit (Leagene, Beijing, China). We centrifuged the cell lysates for supernatants which were stained by Methyl thymol blue solution for 10 min at room temperature. Then the OD values at 610 nm were recorded. Finally, the calcium content was normalized to protein concentrations which were evaluated by a bicinchoninic acid assay kit (Beyotime, Shanghai, China).

Determination of Calcification

To observe the calcification levels of HCASMCs, cells from different groups were collected for fixing with 4% formaldehyde (Solarbio) for 10 min, followed by incubation with 2% alizarin red solution (pH 4.2, Solarbio).

Western Blot Assay

The expression levels of PHGDH, Runx2, bone morphogenetic protein 2 (BMP2), cyclooxygenase 2 (COX2), glutathione peroxidase 4 (GPX4), P53, and solute carrier family 7a member 11 (SLC7A11) were determined by Western blot. Using a 10% sodium dodecyl sulfate-polyacrylamide gel electrophoresis, we separated the proteins extracted from cells which were then transferred from the gel to the polyvinylidene fluoride membrane (Millipore, Danvers, USA). The membrane was exposed to 5% skim milk to be blocked and was then incubated with primary antibodies at 4°C overnight which included anti-PHGDH (ab240744, 1:2000, Abcam), anti-Runx2 (ab236639, 1:1000, Abcam), anti-BMP2 (ab284387, 1:1000, Abcam), anti-COX2 (ab179800, 1:1000, Abcam), anti-GPX4 (ab125066, 1:1000, Abcam), anti-P53 (ab32049, 1:1000, Abcam), anti-SLC7A11 (ab175186, 1:1000, Abcam), and anti-GAPDH (ab181602, 1:10000, Abcam). It was then exposed to Horseradish Peroxidase-conjugated anti-rabbit secondary antibody (ab288151, 1:5000, Abcam) at room temperature for 1 h. Finally, the membranes after exposure were visualized using an electrochemiluminescence detection system (Tanon, Shanghai, China).

Statistical Analysis

Data were presented as multiple groups of repeated data or means ± standard deviation and were processed by GraphPad Prism 7.0 statistical software (GraphPad, San Diego, CA, USA). The comparisons between two groups were determined by Student's t-test, and those among multiple groups were determined by one-way ANOVA with Tukey's post hoc analysis. A p-value less than 0.05 was considered statistically significant.

Results

Identification of DEGs

The GSE211722 dataset was obtained from the GEO database. We selected 3 Control samples (HCASMCs cultured in normal medium) and 3 CAC samples (HCASMCs cultured in osteogenic medium) in the GSE211722 dataset for analysis and the data correction and standardization of the 6 selected samples were achieved through the boxplots (Figure 1A). A total of 201 DEGs were obtained after screening, which were visualized in a volcano plot (Figure 1B) after cluster analysis. The top 3 pathways of gene set enrichment analysis of DEGs were shown in Figure 1C. Finally, we selected the top 15 up-regulated DEGs and the top 15 down-regulated DEGs in GSE211722 (Supplementary Table 2) and visualized them with a heatmap (Figure 1D).

Functional and Pathway Enrichment Analysis

We showed the top 6 items of molecular function MF, biological process BP, and cell component CC of GO enrichment analysis in the bubble diagram (Figure 1E). After KEGG enrichment analysis, the top 8 pathways with the lowest p-value were shown in Figure 1F.

PPI Network Construction and Hub Gene Selection

A PPI network was built based on the interaction information between DEGs (Supplementary Figure 1A). The hub genes were screened out using the plug-ins CytoHubba1 and Molecular Complex Detection in Cytoscape (Supplementary Figure 1B), consisting of PHGDH, SLC6A9, ASNS, TRIB3, SLC7A5, and SLC7A1, which were densely interconnected.

Hub Gene Analysis

The expression changes of hub genes involved in the GO terms were visualized in a chordal graph (Figure 2A) to show the correlation between hub genes and GO terms. The expression ridgeline plot exhibited the distribution of genes in selected sample data (Figure 2B). Using the expression of hub genes in GSE211722 as variables, we performed the PCA and obtained a scatter plot, showing that the two principal components (PC1 and PC2) effectively explained 98.3% of the difference between the control group and the model group (Figure 2C). The matrix analysis revealed the internal correlation of hub genes in GSE211722 (Figure 2D). The ROC curves revealed that taking PHGDH, ASNS, TRIB3, SLC6A9, SLC7A5, and SLC7A1 as indicators in GSE211722, the true positive rates were 88.9%, 77.8%, 88.9%, 77.8%, 88.9%, and 88.9% respectively, indicating that these genes could be used as indicators to distinguish patients with CAC from healthy controls (Supplementary Figure 2).

Expression Analysis of Hub Genes on CAC Model Mice

We determined the expression levels of hub genes in mice from the Control group and the CAC group. The results of H&E staining revealed that in the CAC group, a larger number of punctate or massive plaques appeared around the coronary artery (arrow, Figure 3A). In addition, the vessel wall was thickened, and inflammatory cell infiltration was observed in the CAC group (Figure 3A). The results of Von-Kossa staining showed that there was obvious black calcium deposition in the coronary artery wall (arrow) of the CAC group, while no abnormality in the Control group (Figure 3B). Compared with the Control group, higher expression levels of Runx2 and ALP, the calcification markers, were detected in the CAC group (p<0.01, Figure 3C). The above results proved that our modeling method was feasible and successful. Subsequently, we further confirmed the mRNA expression levels of hub genes in the myocardial tissues and found that compared with the Control group, all of them were significantly decreased in the CAC group (p<0.01, Figure 3D). Based on the current level of research and innovation of each gene, we selected PHGDH for further research. Then we examined the expression level of PHGDH in aortic smooth muscle cells of CAC mice
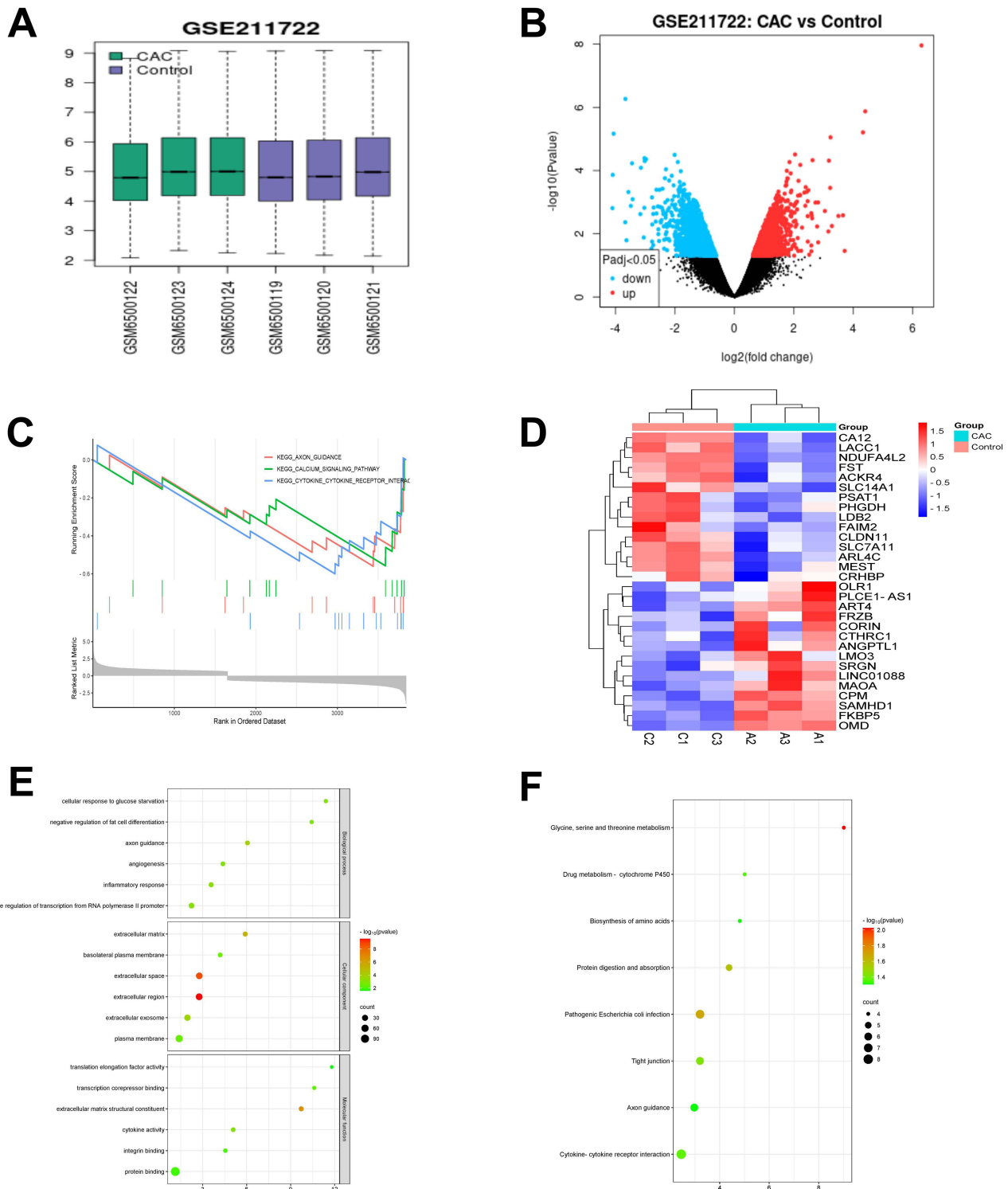
Figure 1 Identification of differentially expressed genes (DEGs). (**A**) A Boxplot showed the data correction results of the selected samples in GSE211722. (**B**) A volcano map of DEGs in GSE211722; red points presented up-regulated DEGs, and blue points presented down-regulated DEGs. CAC: coronary artery calcification. (**C**) The top 3 pathways of gene set enrichment analysis of DEGs in GSE211722. (**D**) The heatmap showed the top 15 up-regulated DEGs and the top 15 down-regulated DEGs in GSE211722. (**E**) A bubble diagram of Gene Ontology enrichment analysis of DEGs. (**F**) A bubble diagram of the Kyoto Encyclopedia of Genes and Genomes pathway analysis of DEGs.

heart tissue by immunofluorescence co-staining of PHGDH and α-SMA and the results of immunofluorescence co-staining showed that compared with the Control group, the expression level of PGDGH in α-SMA positive aera in the CAC group was decreased (Figure 3E).
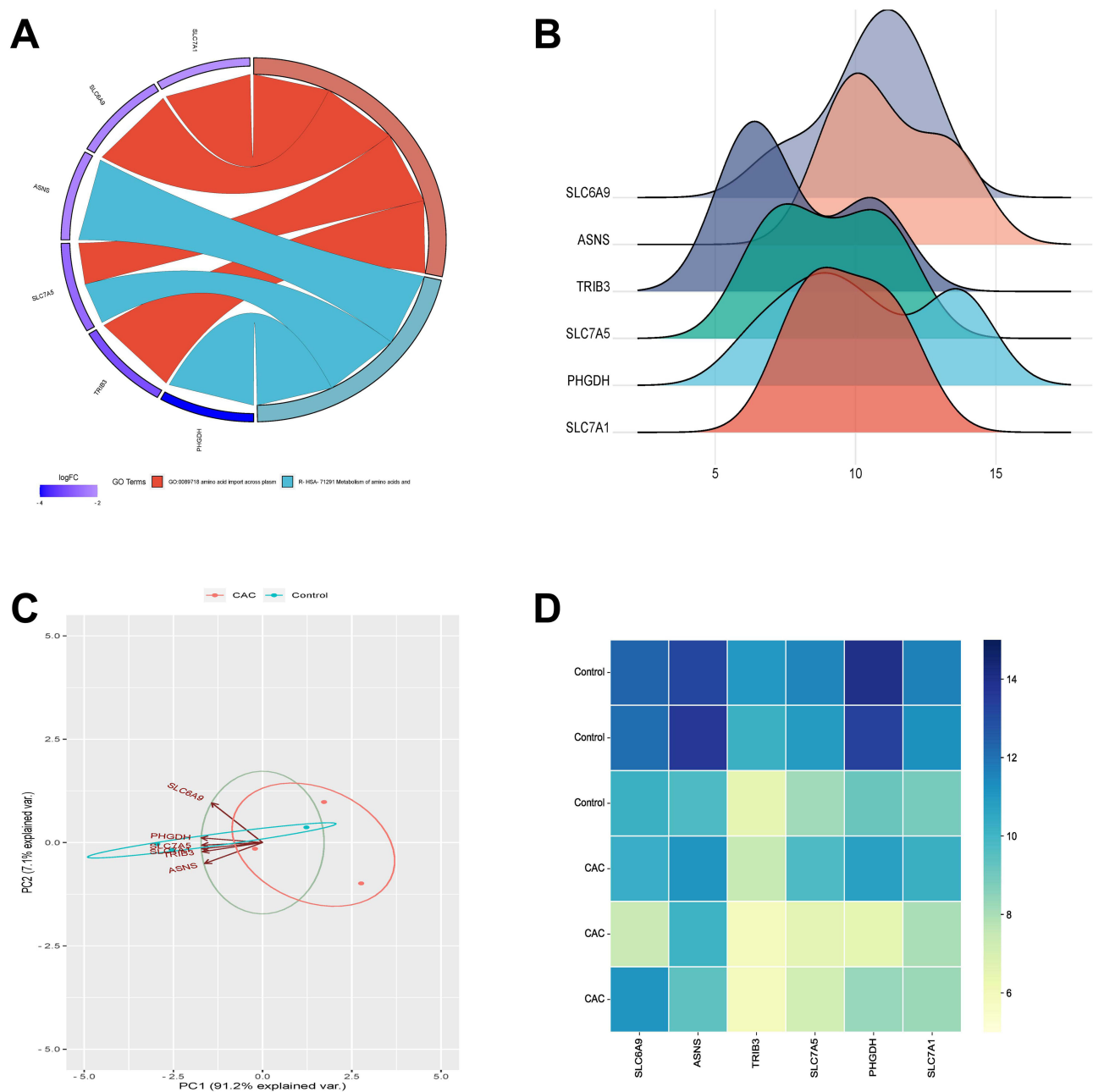
Figure 2 Hub gene analysis. (**A**) A chordal graph. (**B**) A ridgeline plot. (**C**) The principal component analysis. (**D**) The matrix analysis.

Overexpression of PHGDH Inhibits the Calcification Level of CM-Induced HCASMCs

We examined the transfection efficiency of pcDNA3.1-PHGDH by RT-qPCR and Western blotting and found that pcDNA3.1-PHGDH transfection significantly increased the relative mRNA and protein expression levels of PHGDH in HCASMCs ($p<0.01$, Figure 4A). Subsequently, excepted for the Normal group, all cells in each group were treated with CM. We observed that PHGDH overexpression significantly elevated the cell viability, which was reduced by CM ($p<0.01$, Figure 4B). The results of alizarin red staining showed a lower calcification level in the oe-PHGDH group and a higher level in the Control group or the oe-NC group (Figure 4C). Compared with the oe-NC group, there were lower expression levels of RUNX2, BMP2, ALP, and calcium in the oe-PHGDH group ($p<0.01$, Figure 4D–F).
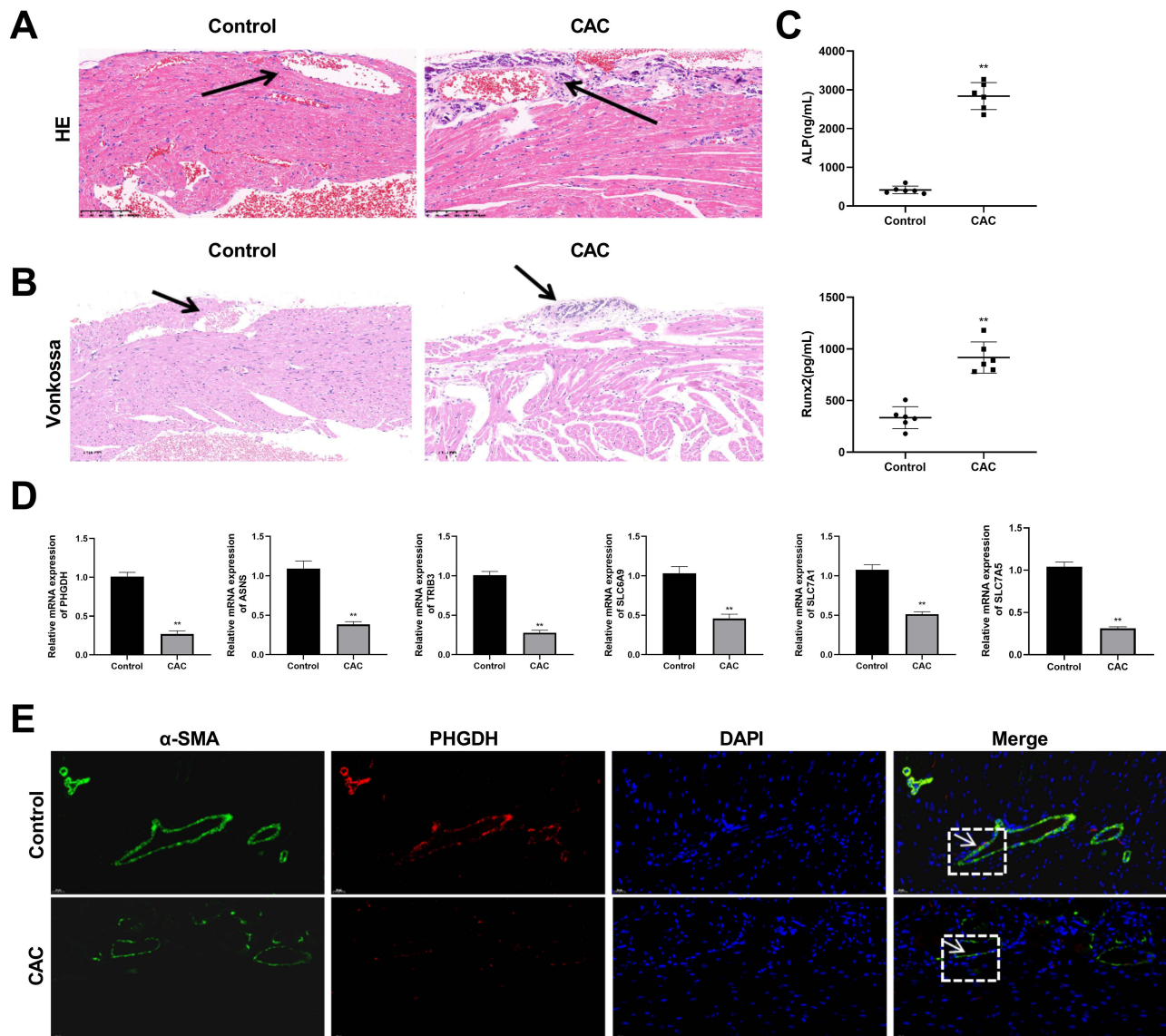
Figure 3 The expression validation of hub genes. (**A**) The results of Hematoxylin-eosin (HE) staining (200×). Scale bars=100 μm. Arrows pointed to the coronary artery. (**B**) The results of Von-Kossa staining (200×). Scale bars=100 μm. Arrows pointed to the coronary artery. (**C**) The expression levels of the calcification markers in the serum of mice. ALP: relative alkaline phosphatase; RUNX2: runt-related transcription factor 2. (**D**) The relative mRNA expression levels of hub genes. PHGDH: Phosphoglycerate dehydrogenase; ASNS: asparagine synthetase; TRIB3: tribbles homologue 3; SLC6A9: solute carrier family 6 member 9; SLC7A1: solute carrier family 7 member 1; SLC7A5: solute carrier family 7 member 5. (**E**) The results of immunofluorescence co-staining of PHGDH and α-smooth muscle actin (α-SMA) (400×). The positions where the co-expression differences were significant were shown in the white boxes. Scale bars=20 μm. DAPI: 4',6-diamidino-2-phenylindole. **$p < 0.01$ vs the Control group.

Inhibition of Ferroptosis Suppresses the Calcification Level of CM-Induced HCASMCs

Compared with the Control group, the calcification level determined by alizarin red staining was decreased, which was induced by CM (Figure 5A). The expression levels of calcium, BMP2, and Runx2 were significantly elevated by CM, while were all suppressed by Fer-1 (all $p<0.01$, Figure 5B and C). Then, we detected the ferroptosis-related indicators in each group. Compared with the Normal group, lower levels of GSH and GPX4 and a higher level of COX2 were found in the Control group (all $p<0.01$, Figure 5D and E), showing that ferroptosis was induced by CM. Compared with the Control group, Fer-1 successfully suppressed ferroptosis based on the increased levels of GSH and GPX4 and the reduced level of COX2 (all $p<0.01$, Figure 5D and E). The above results indicated that inhibition of ferroptosis could restrain the calcification level of HCASMCs.
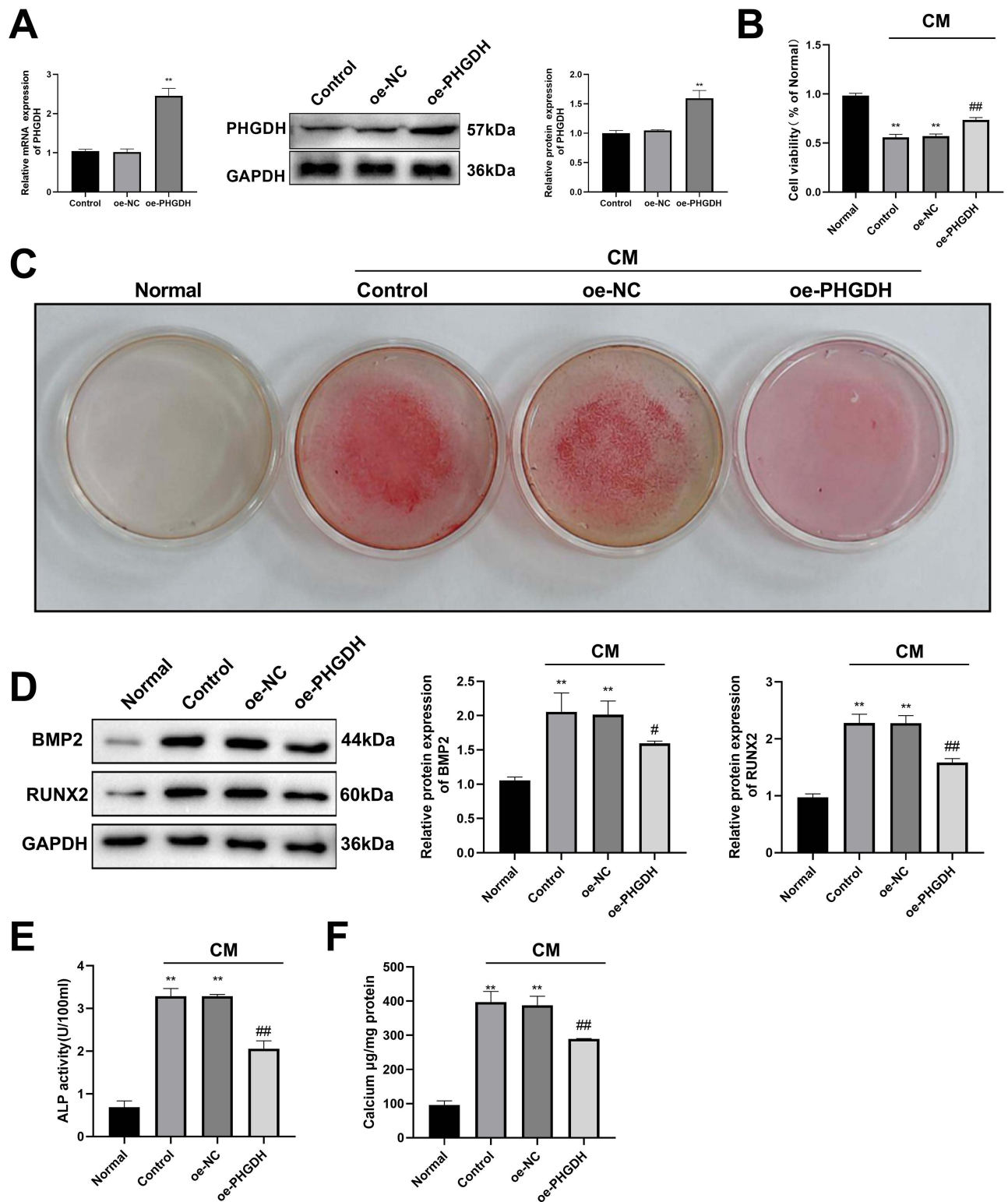
Figure 4 PHGDH overexpression inhibited the calcification level of calcifying medium (CM)-induced human coronary artery smooth muscle cells (HCASMCs). (**A**) The relative mRNA and protein expression levels of PHGDH. (**B**) The cell viability. (**C**) The results of alizarin red staining. (**D**) The protein expression level of RUNX2 and bone morphogenetic protein 2 (BMP2). (**E**) The relative ALP activity. (**F**) The calcium content. **$p < 0.01$ vs the Normal group; ##$p < 0.01$ vs the oe-NC group.
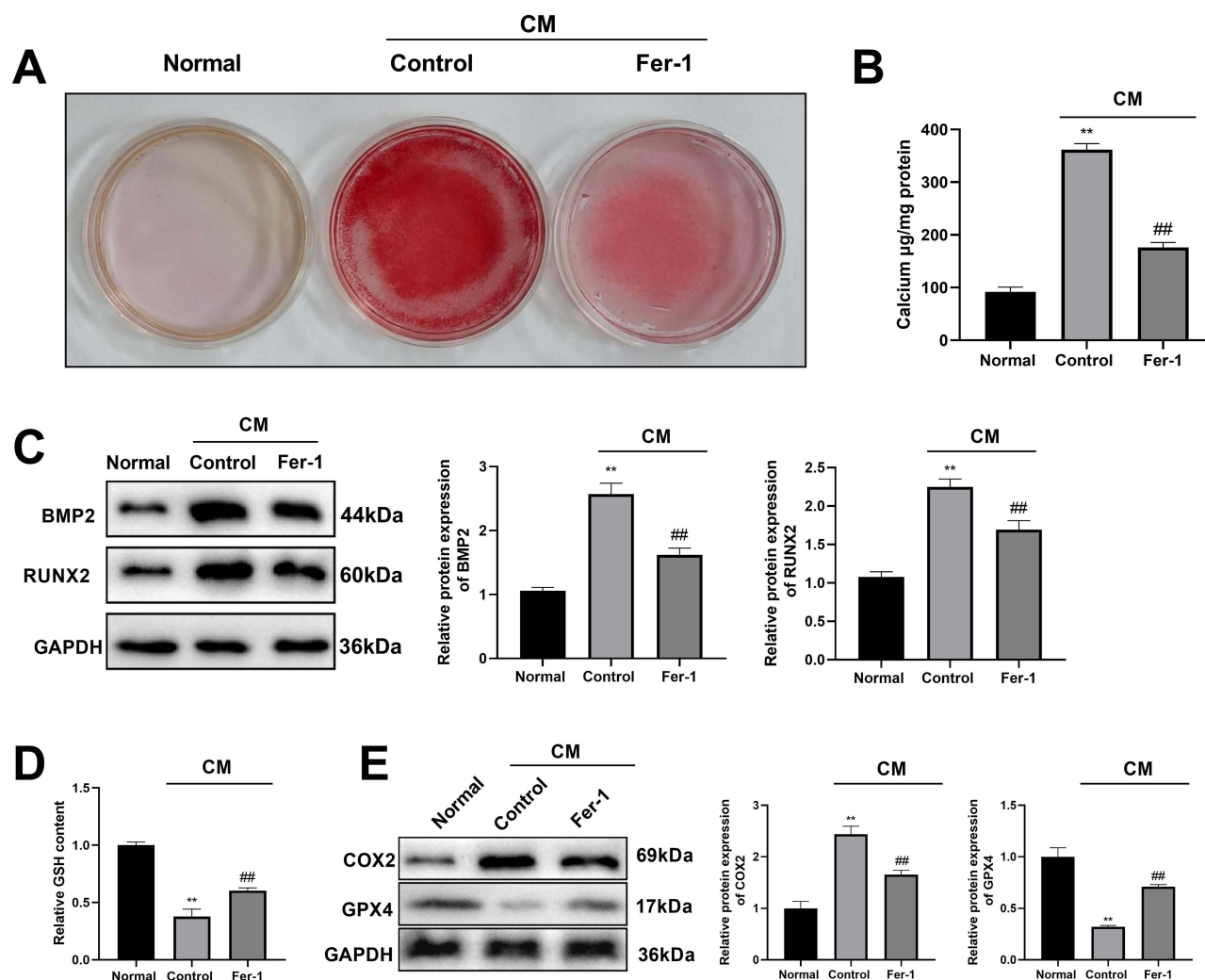
Figure 5 Inhibition of ferroptosis suppressed the calcification level of CM-induced HCASMCs. (**A**) The results of alizarin red staining. Fer-1: ferrostatin-1. (**B**) The calcium content. (**C**) The protein expression level of RUNX2 and BMP2. (**D**) The expression level of glutathione (GSH). (**E**) The protein expression levels of cyclooxygenase 2 (COX2) and glutathione peroxidase 4 (GPX4). **$p < 0.01$ vs the Normal group; ##$p < 0.01$ vs the Control group.

Overexpression of PHGDH Inhibits the Calcification Level of CM-Induced HCASMCs by Inhibiting Ferroptosis

We further explored the role of PHDGH in the calcification of HCASMCs using Erastin, an inducer of ferroptosis. Excepted for the Normal group, all cells in each group were treated with CM. Compared with the Normal group, the calcification level determined by alizarin red staining was induced by CM in the oe-NC group, which was further elevated by Erastin (Figure 6A). Compared with the oe-NC group, PHGDH overexpression suppressed the calcification level, which was reversed by Erastin (Figure 6A). Similarly, PHGDH overexpression significantly suppressed the expression level of calcium and the ALP activity, which were all reversed by Erastin (all $p<0.01$, Figure 6B and C), indicating a correlation between PHGDH overexpression and ferroptosis. Therefore, we determined the expression levels of GSH, COX2, and GPX4. Compared with the Normal group, the levels of GSH and GPX4 were suppressed by CM, which were further decreased by Erastin (all $p<0.01$, Figure 6D and E), and the level of COX2 was increased by CM, which was further induced by Erastin (all $p<0.01$, Figure 6E). Compared with the oe-NC group, PHGDH overexpression increased the levels of GSH and GPX4 and decreased the level of COX2 (Figure 6D and E). Compared with the oe-PHGDH group, lower levels of GSH and GPX4 and a higher level of COX2 were found in the oe-PHGDH + Erastin group (all $p<0.01$, Figure 6D and E).
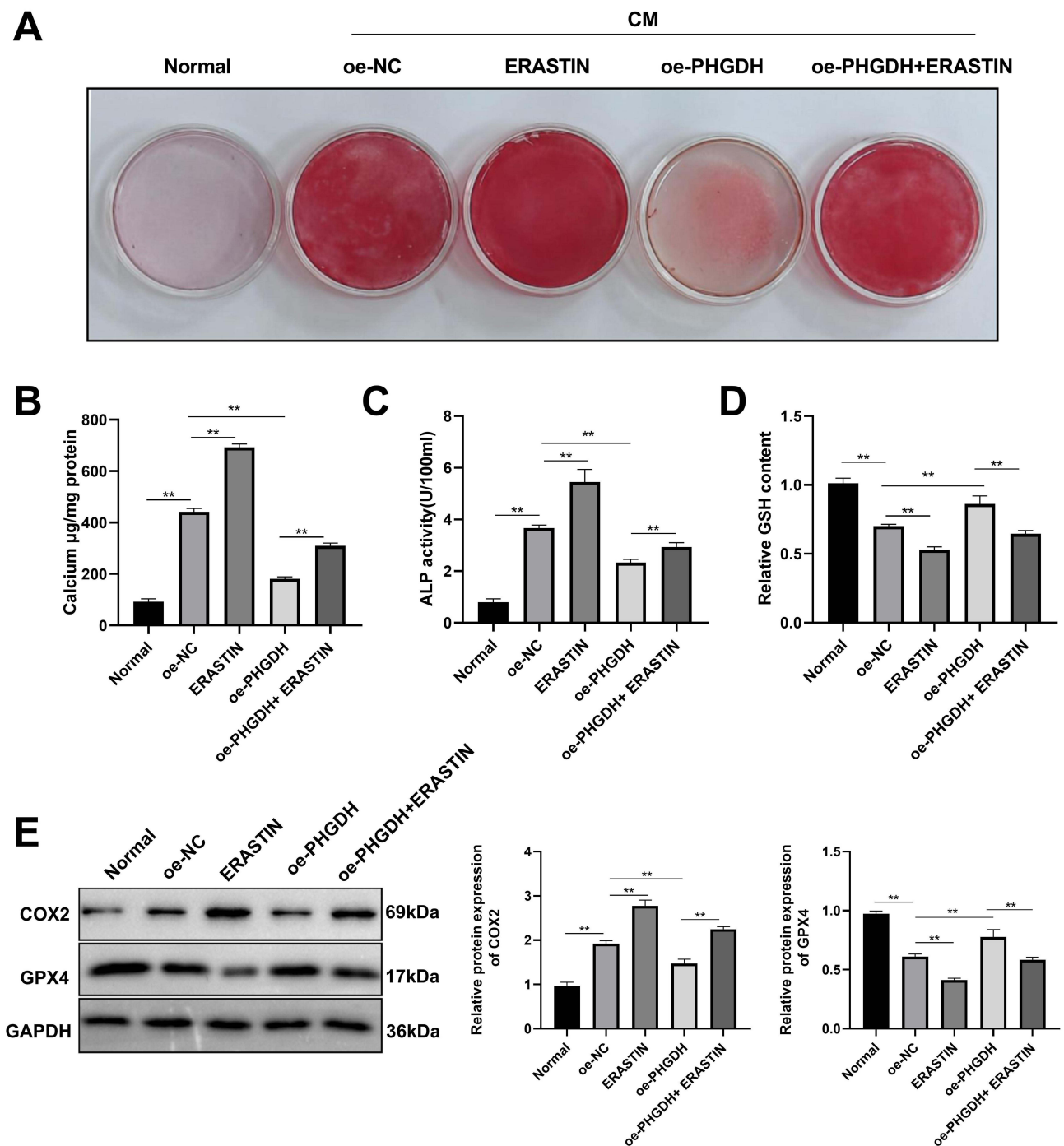
Figure 6 PHGDH overexpression inhibited the calcification level of CM-induced HCASMCs by inhibiting ferroptosis. (**A**) The results of alizarin red staining. (**B**) The calcium content. (**C**) The relative ALP activity. (**D**) The expression level of GSH. (**E**) The protein expression level of COX2 and GPX4. **$p < 0.01$.

Overexpression of PHGDH Inhibits HCASMC Calcification by Regulating the P53/ SLC7A11 Signaling Pathway

To further reveal the regulatory mechanism of PHGDH in HCASMC calcification, we determined the protein expression of P53 and SLC7A11. Up-regulation of PHGDH could restrain the level of P53 and promote the level of SLC7A11 ($p<0.01$, Figure 7A). On the contrary, down-regulation of PHGDH could increase the expression level of P53 and reduce
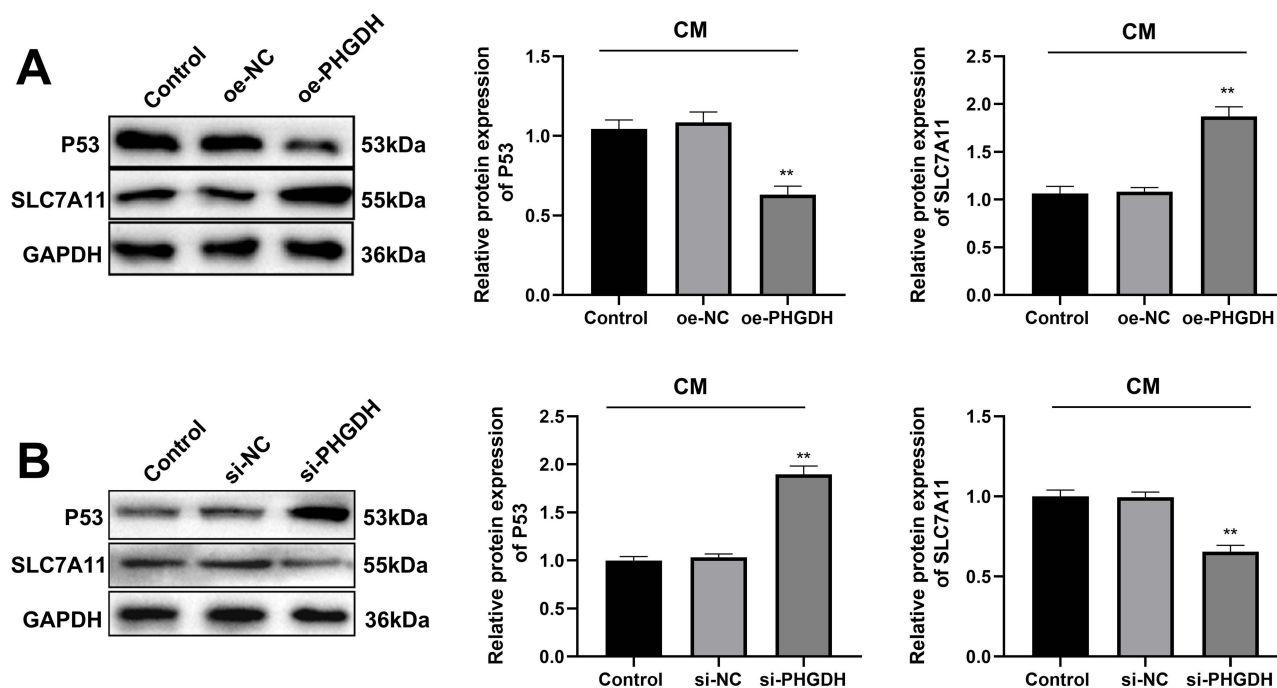
Figure 7 The effect of PHGDH on the expression of P53 and Solute carrier family 7a member 11 (SLC7A11). (**A**) PHGDH overexpression inhibited P53 protein expression and increased SLC7A11 protein expression; **p < 0.01 vs the oe-NC group. (**B**) Silencing PHGDH increased P53 protein expression and suppressed SLC7A11 protein expression; **p < 0.01 vs the si-NC group.

the level of SLC7A11 ($p<0.01$, Figure 7B), indicating that PHGDH suppressed HCASMC calcification by regulating the P53/SLC7A11 signaling pathway.

Discussion

CAC is present in almost all patients with coronary artery disease, relevant to vascular injury, inflammation, and repair, with few definitive pharmacological interventions available.[1] It is meaningful to search for effective biomarkers for the diagnosis and treatment of CAC. In our study, six hub genes, namely PHGDH, SLC6A9, ASNS, TRIB3, SLC7A5, and SLC7A1, were screened out by bioinformatics analysis. Then, we selected PHGDH and explored its potential effects on CAC. Finally, we found that PHGDH overexpression inhibited the calcification level of CM-induced HCASMCs by suppressing ferroptosis through the P53/SLC7A11 signaling pathway.

Calcium, the most abundant mineral in the human body, approximately 1% is dissolved in the bloodstream,[1] which can be identified with the assistance of Von-Kossa and alizarin red staining.[28] Calcification has been reported to be an active and regulated process, similar to that of bone formation, accompanied by a train of changes including ALP activation and elevated expression of osteogenesis-related proteins such as BMP2 and Runx2.[29] ALP is involved in the process of mineral metabolism and is a molecular marker for vascular calcification.[30] Ren et al have reported that the levels of ALP in serum are related to plaque vulnerability and the patterns of CAC.[31] BMP2, a kind of pluripotent factor, can regulate the ALP activity.[32] Interleukin-29 promotes vascular calcification by increasing the expression of BMP2.[33] Samanta J et al have reported that the calcification of cardiomyocytes depends on the Forkhead Box Protein O1/ Nuclear factor of activated T cells 3/Runx2 axis.[34] C1q/ tumor necrosis factor-related protein-13 accelerates the degradation of Runx2, alleviating vascular calcification.[35] In this research, we observed a decreased level of RUNX2, BMP2, ALP activity, calcium content, and calcification level in CM-induced HCASMCs with overexpression of PHGDH, indicating PHGDH overexpression could inhibit calcification of HCASMCs.

PHGDH, ASNS, TRIB3, SLC7A5, and SLC7A1 have been found to be associated with ferroptosis.[20,36–39] Although the role of ferroptosis in CAC is not clear, there is a growing body of research that links ferroptosis to vascular calcification. Ye et al have observed that ferroptosis induction can promote the progression of vascular

calcification.[40] Down-regulation of Fos-like antigen 1 reduces the ferroptosis with the attenuation of vascular calcification.[41] Therefore, we further investigated whether PHGDH could regulate the ferroptosis in CAC. Ferroptosis is accompanied by an increased expression of the positive regulators, such as COX2, and a decreased expression of the negative regulators, such as GPX4.[42,43] Cell membranes containing phospholipids are under reactive oxygen attack due to the consumption of GSH and the impaired antioxidant capacity of GPX4.[44] In our study, we found an elevated expression of GPX4 and GSH and a reduced expression of COX2 in CM-induced HCASMCs with overexpression of PHGDH, which were all reversed by Erastin, suggesting that overexpression of PHGDH inhibited the calcification level by inhibiting ferroptosis.

P53 is a known important regulator of ferroptosis.[45] SLC7A11, a kind of cystine transporter, is a target gene of P53.[45] When p53 is activated, the expression level of SLC7A11 will be severely decreased.[45] The signal transducer and activator of transcription 6 attenuates acute lung injury by suppressing ferroptosis via the P53/SLC7A11 pathway.[46] Shank-associated RH domain interacting protein plays a role in stimulating cell proliferation of cholangiocarcinoma with suppression of ferroptosis through the P53/SLC7A11/GPX4 pathway.[47] Overexpression of ubiquitin-specific protease 22 inhibits the ferroptosis of cardiomyocytes by the P53/SLC7A11 signaling, reducing cardiomyocyte death and alleviating myocardial ischemia-reperfusion injury.[48] In addition, P53 signaling can regulate mitochondrial dynamics in vascular smooth muscle cell calcification.[49] Suppression of SLC7A11/GSH/GPX4 axis promotes ferroptosis and vascular calcification.[40] Down-regulation of Fos-like antigen 1 protects against vascular calcification with ferroptosis inhibition by P53/SLC7A11 signaling pathway.[41] Accumulating studies have shown that there is an interaction between P53 and PHGDH. Wu et al have reported that PHGDH is a p53-binding protein and participates in the formation of p53-binding complexes.[50] In human melanoma cells, P53 can suppress PHGDH expression to promote the apoptotic response.[51] Wang J et al have found that inhibition of PHGDH triggers ferroptosis by up-regulating P53 and suppressing SLC7A11, overcoming enzalutamide resistance in castration-resistant prostate cancer cells.[12] In this study, we found that up-regulation of PHGDH could restrain the expression of P53 and promote the expression of SLC7A11, indicating that PHGDH overexpression inhibited HCASMC calcification by regulating the P53/SLC7A11 signaling pathway. The potential mechanism of PHGDH overexpression inhibiting P53 needs to be investigated in the future.

In conclusion, PHGDH was finally screened out by bioinformatic analysis. PHGDH overexpression could suppress the calcification of HCASMCs by inhibiting ferroptosis through the P53/SLC7A11 signaling pathway, suggesting PHGDH as a possible therapeutic target of CAC.

Data Sharing Statement

The data that support the findings of this study are openly available in Gene Expression Omnibus at https://www.ncbi.nlm.nih.gov, reference number GSE211722.

Ethics Approval and Consent to Participate

All animal experimental procedures were performed with the approval of the Southern Theater Command General Hospital (Approval No.: SYDW2023070). Since our experiment did not involve human clinical research and only used purchased HCASMCs, human ethical approval was not required.

Author Contributions

All authors made a significant contribution to the work reported, whether that is in the conception, study design, execution, acquisition of data, analysis, and interpretation, or in all these areas; took part in drafting, revising, or critically reviewing the article; gave final approval of the version to be published; have agreed on the journal to which the article has been submitted; and agree to be accountable for all aspects of the work.

Funding

Disclosure

The authors declare that they have no conflicts of Interest in this work.

References

1. Mohan J. *Coronary Artery Calcification*, in *StatPearls*. 2023, StatPearls Publishing Copyright © 2023, StatPearls Publishing LLC.: Treasure Island (FL) ineligible companies. Disclosure: Karan Bhatti declares no relevant financial relationships with ineligible companies. Disclosure: Adam Tawney declares no relevant financial relationships with ineligible companies. Disclosure: Roman Zeltser declares no relevant financial relationships with ineligible companies.
2. Mori H, Torii S, Kutyna M, et al. Coronary artery calcification and its progression: what does it really mean? *JACC Cardiovasc*. 2018;11 (1):127–142. doi:10.1016/j.jcmg.2017.10.012
3. Patel J, Pallazola VA, Dudum R, et al. Assessment of coronary artery calcium scoring to guide statin therapy allocation according to risk-enhancing factors: the multi-ethnic study of atherosclerosis. *JAMA Cardiol*. 2021;6(10):1161–1170. doi:10.1001/jamacardio.2021.2321
4. Nakanishi R, Li D, Blaha MJ, et al. The relationship between coronary artery calcium score and the long-term mortality among patients with minimal or absent coronary artery risk factors. *Int J Cardiol*. 2015;185:275–281. doi:10.1016/j.ijcard.2015.03.146
5. Knapper JT, Khosa F, Blaha MJ, et al. Coronary calcium scoring for long-term mortality prediction in patients with and without a family history of coronary disease. *Heart*. 2016;102(3):204–208. doi:10.1136/heartjnl-2015-308429
6. Rheude T, Fitzgerald S, Allali A, et al. Rotational atherectomy or balloon-based techniques to prepare severely calcified coronary lesions. *JACC*. 2022;15(18):1864–1874. doi:10.1016/j.jcin.2022.07.034
7. Lee MS, Gordin JS, Stone GW, et al. Orbital and rotational atherectomy during percutaneous coronary intervention for coronary artery calcification. *Catheter Cardiovasc Interv*. 2018;92(1):61–67. doi:10.1002/ccd.27339
8. Rossi M, Altea-Manzano P, Demicco M, et al. PHGDH heterogeneity potentiates cancer cell dissemination and metastasis. *Nature*. 2022;605 (7911):747–753. doi:10.1038/s41586-022-04758-2
9. Wang K, Luo L, Fu S, et al. PHGDH arginine methylation by PRMT1 promotes serine synthesis and represents a therapeutic vulnerability in hepatocellular carcinoma. *Nat Commun*. 2023;14(1):1011. doi:10.1038/s41467-023-36708-5
10. Zhang D, Li AM, Hu G, et al. PHGDH-mediated endothelial metabolism drives glioblastoma resistance to chimeric antigen receptor T cell immunotherapy. *Cell Metab*. 2023;35(3):517–534.e8. doi:10.1016/j.cmet.2023.01.010
11. Wei L, Lee D, Law C-T, et al. Genome-wide CRISPR/Cas9 library screening identified PHGDH as a critical driver for Sorafenib resistance in HCC. *Nat Commun*. 2019;10(1):4681. doi:10.1038/s41467-019-12606-7
12. Wang J, Zeng L, Wu N, et al. Inhibition of phosphoglycerate dehydrogenase induces ferroptosis and overcomes enzalutamide resistance in castration-resistant prostate cancer cells. *Drug Resist Updat*. 2023;70:100985. doi:10.1016/j.drup.2023.100985
13. Chen X, Calandrelli R, Girardini J, et al. PHGDH expression increases with progression of Alzheimer's disease pathology and symptoms. *Cell Metab*. 2022;34(5):651–653. doi:10.1016/j.cmet.2022.02.008
14. Huang H, Liu K, Ou H, et al. Phgdh serves a protective role in Il-1β induced chondrocyte inflammation and oxidative-stress damage. *Mol Med Rep*. 2021;23(6). doi:10.3892/mmr.2021.12058
15. Perea-Gil I, Seeger T, Bruyneel AAN, et al. Serine biosynthesis as a novel therapeutic target for dilated cardiomyopathy. *Eur Heart J*. 2022;43 (36):3477–3489. doi:10.1093/eurheartj/ehac305
16. Truong V, Huang S, Dennis J, et al. Blood triglyceride levels are associated with DNA methylation at the serine metabolism gene PHGDH. *Sci Rep*. 2017;7(1):11207. doi:10.1038/s41598-017-09552-z
17. Wu Y, Tang L, Huang H, et al. Phosphoglycerate dehydrogenase activates PKM2 to phosphorylate histone H3T11 and attenuate cellular senescence. *Nat Commun*. 2023;14(1):1323. doi:10.1038/s41467-023-37094-8
18. Jiang X, Stockwell BR, Conrad M. Ferroptosis: mechanisms, biology and role in disease. *Nat Rev Mol Cell Biol*. 2021;22(4):266–282. doi:10.1038/s41580-020-00324-8
19. Mou Y, Wang J, Wu J, et al. Ferroptosis, a new form of cell death: opportunities and challenges in cancer. *J Hematol Oncol*. 2019;12(1):34. doi:10.1186/s13045-019-0720-y
20. Shen L, Zhang J, Zheng Z, et al. PHGDH Inhibits ferroptosis and promotes malignant progression by upregulating SLC7A11 in bladder cancer. *Int J Biol Sci*. 2022;18(14):5459–5474. doi:10.7150/ijbs.74546
21. You J, Ouyang S, Xie Z, et al. The suppression of hyperlipid diet-induced ferroptosis of vascular smooth muscle cells protests against atherosclerosis independent of p53/SCL7A11/GPX4 axis. *J Cell Physiol*. 2023;238(8):1891–1908. doi:10.1002/jcp.31045
22. Li Y, Feng D, Wang Z, et al. Ischemia-induced ACSL4 activation contributes to ferroptosis-mediated tissue injury in intestinal ischemia/ reperfusion. *Cell Death Differ*. 2019;26(11):2284–2299. doi:10.1038/s41418-019-0299-4
23. Ta N, Qu C, Wu H, et al. Mitochondrial outer membrane protein FUNDC2 promotes ferroptosis and contributes to doxorubicin-induced cardiomyopathy. *Proc Natl Acad Sci U S A*. 2022;119(36):e2117396119. doi:10.1073/pnas.2117396119
24. Peng C, Zhang Y, Lang X, et al. Role of mitochondrial metabolic disorder and immune infiltration in diabetic cardiomyopathy: new insights from bioinformatics analysis. *J Transl Med*. 2023;21(1):66. doi:10.1186/s12967-023-03928-8
25. Liu F, Wei T, Liu L, et al. Role of necroptosis and immune infiltration in human Stanford type a aortic dissection: novel insights from bioinformatics analyses. *Oxid Med Cell Longev*. 2022;2022:6184802. doi:10.1155/2022/6184802
26. Pan H, Xue C, Auerbach BJ, et al. Single-cell genomics reveals a novel cell state during smooth muscle cell phenotypic switching and potential therapeutic targets for atherosclerosis in mouse and human. *Circulation*. 2020;142(21):2060–2075. doi:10.1161/CIRCULATIONAHA.120.048378
27. De Maré A, Opdebeeck B, Neven E, et al. Sclerostin protects against vascular calcification development in mice. *J Bone Miner Res*. 2022;37 (4):687–699. doi:10.1002/jbmr.4503
28. Wang PW, Pang Q, Zhou T, et al. Irisin alleviates vascular calcification by inhibiting VSMC osteoblastic transformation and mitochondria dysfunction via AMPK/Drp1 signaling pathway in chronic kidney disease. *Atherosclerosis*. 2022;346:36–45. doi:10.1016/j.atherosclerosis.2022.02.007
29. Wang Y, Hu Y-C, Zhou Y, et al. Relationship between coronary artery calcification and calcium deposition in the myocardium. *J Int Med Res*. 2019;47(7):2910–2920. doi:10.1177/0300060519848587

30. Johnson RC, Leopold JA, Loscalzo J. Vascular calcification: pathobiological mechanisms and clinical implications. *Circ Res*. 2006;99 (10):1044–1059. doi:10.1161/01.RES.0000249379.55535.21

31. Ren Y, Li X, Wang S, et al. Serum alkaline phosphatase levels are associated with coronary artery calcification patterns and plaque vulnerability. *Catheter Cardiovasc Interv*. 2021;97(Suppl 2):1055–1062. doi:10.1002/ccd.29642

32. Kong Y, Liang Q, Chen Y, et al. Hyaluronan negatively regulates vascular calcification involving BMP2 signaling. *Lab Invest*. 2018;98 (10):1320–1332. doi:10.1038/s41374-018-0076-x

33. Hao N, Zhou Z, Zhang F, et al. Interleukin-29 accelerates vascular calcification via JAK2/STAT3/BMP2 Signaling. *J Am Heart Assoc*. 2023;12(1): e027222. doi:10.1161/JAHA.122.027222

34. Samanta J, Mondal A, Das S, et al. Induction of cardiomyocyte calcification is dependent on FoxO1/NFATc3/Runx2 signaling. *Vitro Cell Dev Biol Anim*. 2021;57(10):973–986. doi:10.1007/s11626-021-00623-0

35. Li Y, Wang W, Chao Y, et al. CTRP13 attenuates vascular calcification by regulating Runx2. *FASEB j*. 2019;33(8):9627–9637. doi:10.1096/fj.201900293RRR

36. Shen C, Wang Y. Ferroptosis biomarkers for predicting prognosis and immunotherapy efficacy in adrenocortical carcinoma. *Arch Med Res*. 2023;54 (1):45–55. doi:10.1016/j.arcmed.2022.12.003

37. Yuan Z, Liu T, Huo X, et al. Glutamine transporter SLC1A5 regulates ionizing radiation-derived oxidative damage and ferroptosis. *Oxid Med Cell Longev*. 2022;2022:3403009. doi:10.1155/2022/3403009

38. Wang B, Fu C, Wei Y, et al. Ferroptosis-related biomarkers for Alzheimer's disease: identification by bioinformatic analysis in hippocampus. *Front Cell Neurosci*. 2022;16:1023947. doi:10.3389/fncel.2022.1023947

39. Wu X, Qin K, Iroegbu CD, et al. Genetic analysis of potential biomarkers and therapeutic targets in ferroptosis from coronary artery disease. *J Cell Mol Med*. 2022;26(8):2177–2190. doi:10.1111/jcmm.17239

40. Ye Y, Chen A, Li L, et al. Repression of the antiporter SLC7A11/glutathione/glutathione peroxidase 4 axis drives ferroptosis of vascular smooth muscle cells to facilitate vascular calcification. *Kidney Int*. 2022;102(6):1259–1275. doi:10.1016/j.kint.2022.07.034

41. Shao S, Liu Y, Hong W, et al. Influence of FOSL1 inhibition on vascular calcification and ros generation through ferroptosis via p53-slc7a11 axis. *Biomedicines*. 2023;11(2):635. doi:10.3390/biomedicines11020635

42. Hu ZW, Wen Y-H, Ma R-Q, et al. Ferroptosis driver SOCS1 and suppressor FTH1 independently correlate with M1 and M2 macrophage infiltration in head and neck squamous cell carcinoma. *Front Cell Dev Biol*. 2021;9:727762. doi:10.3389/fcell.2021.727762

43. Lee J, Roh JL. Induction of ferroptosis in head and neck cancer: a novel bridgehead for fighting cancer resilience. *Cancer Lett*. 2022;546:215854. doi:10.1016/j.canlet.2022.215854

44. Li D, Wang Y, Dong C, et al. CST1 inhibits ferroptosis and promotes gastric cancer metastasis by regulating GPX4 protein stability via OTUB1. *Oncogene*. 2023;42(2):83–98. doi:10.1038/s41388-022-02537-x

45. Liu Y, Gu W. p53 in ferroptosis regulation: the new weapon for the old guardian. *Cell Death Differ*. 2022;29(5):895–910. doi:10.1038/s41418-022-00943-y

46. Yang Y, Ma Y, Li Q, et al. STAT6 inhibits ferroptosis and alleviates acute lung injury via regulating P53/SLC7A11 pathway. *Cell Death Dis*. 2022;13(6):530. doi:10.1038/s41419-022-04971-x

47. Zeng C, Lin J, Zhang K, et al. SHARPIN promotes cell proliferation of cholangiocarcinoma and inhibits ferroptosis via p53/SLC7A11/GPX4 p53/SLC7A11 / GPX4 signaling. *Cancer Sci*. 2022;113(11):3766–3775. doi:10.1111/cas.15531

48. Ma S, Sun L, Wu W, et al. USP22 protects against myocardial ischemia-reperfusion injury via the SIRT1-p53/SLC7A11-dependent inhibition of ferroptosis-induced cardiomyocyte death. *Front Physiol*. 2020;11:551318. doi:10.3389/fphys.2020.551318

49. Phadwal K, Tang Q-Y, Luijten I, et al. p53 regulates mitochondrial dynamics in vascular smooth muscle cell calcification. *Int J Mol Sci*. 2023;24 (2):1643. doi:10.3390/ijms24021643

50. Wu YQ, Zhang C-S, Xiong J, et al. Low glucose metabolite 3-phosphoglycerate switches PHGDH from serine synthesis to p53 activation to control cell fate. *Cell Res*. 2023;33(11):835–850. doi:10.1038/s41422-023-00874-4

51. Ou Y, Wang S-J, Jiang L, et al. p53 Protein-mediated regulation of phosphoglycerate dehydrogenase (PHGDH) is crucial for the apoptotic response upon serine starvation. *J Biol Chem*. 2015;290(1):457–466. doi:10.1074/jbc.M114.616359